Journal of Materials Chemistry B

Accepted Manuscript

ROYAL SOCIETY OF CHEMISTRY

www.rsc.org/materialsB

Enhanced osteoblast differentiation and osseointegration of a bio-inspired HA nanorods patterned pores-sealed MgO bilayer coating on magnesium

Bo Li [1], Yong Han [1*], Mei Li [1, 2]

1. State Key Laboratory for Mechanical Behavior of Materials, Xi'an Jiaotong University, Xi'an 710049, China.

2. Hospital of Orthopedics, Guangzhou General Hospital of Guangzhou Military Command, Guangzhou 510010, China.

Abstract

Endosseous magnesium (Mg) and its alloy implants are meeting obstacle due to their fast degradation and resultant poor cytocompatibility and osseointegration. Herein, a bio-inspired coating (named as HT24h), comprising an outer layer of narrow interrod spaced hydroxyapatite (HA) nanorods mimicking the osteoclasts-created nanotopography of bone matrix at remodeling sites and an inner layer of pores-sealed MgO, was fabricated on Mg using microarc oxidation (MAO) and hydrothermal treatment (HT). Its effects on *in vitro* hFOB1.19 cell functions such as proliferation, differentiation and extracellular matrix mineralization as well as *in vivo* osteogenesis, bone-implant contact, push-out force and pushed-out failure mode assessed osseointegration were investigated, together with porous MgO (MAO_0)- and MgO

* Corresponding author: yonghan@mail.xjtu.edu.cn (Y. Han).Tel.:+86 02982665580; fax: +86 02982663453

containing $Mg(OH)_2$-sealing-pores (HT2h)-coated Mg. Compared to MAO_0- and HT2h-coated Mg, HT24h-coated Mg greatly enhanced osteoblast functions, which ascribed to the HA nanorods derived up-regulated intracellular Ca^{2+} and down-regulated intracellular Mg^{2+} concentrations as well as the lightened H_2 evolution and alkalization of surrounding medium. Owing to the enhanced osteoblast functions, HT24h-coated Mg greatly enhanced osseointegration and its pushed-out failure occurred predominantly within the peri-implant bone rather than within the coating for HT2h-coated Mg and at the coating/Mg interface for MAO_0-coated Mg, giving rise to an advanced Mg-based implant with improved clinical performance.

Keywords: magnesium-based implant, bio-inspired coating, osteoblast, differentiation, osseointegration

1. Introduction

Magnesium (Mg) and its alloys have been widely investigated as candidate biomaterials for orthopedic applications, owing to their biodegradability, high mechanical strength, and low toxicity. Moreover, Mg alloys are smaller in elastic modulus than conventional orthopedic implant materials such as Ti alloys and match well to that of nature bone. As a result, it can reduce the stress-shielding effect which leads to reduced simulation of new bone growth and remodeling. However, clinical applications of Mg alloys are currently meeting obstacle due to their fast degradation in physiological environments and consequent loss of their mechanical integrity.[1]

Furthermore, the hydrogen accumulation and strong alkalization of the surrounding body fluid during fast degradation of Mg alloys would damage the cells and inhibit new bone formation.[2-4] To overcome the demerits, two strategies are tried: one is tailoring the microstructure of Mg alloys, such as composition by alloying,[5] grain refinement by equal channel angular pressing,[6] amorphization by rapid solidification,[7] and refinement and dispersion of the second phase by high-ratio rolling;[8] the other is surface modification, to produce protective ceramic, polymer or composite coatings on Mg alloys. Both of them can, to certain extent, reduce degradation of Mg alloys *in vitro* or *in vivo*, however, surface modification is of significance in enhancing corrosion resistance.[5,9,10]

Most importantly, cytocompatibility and osseointegration are also crucial concerns involved in Mg-based bone implants, as given that the bare ones exhibited high cell mortality and fibrous capsule.[11,12] Alternatively, surface modification of Mg alloys with coatings improved the biological performance. For instance, micro-arc oxidation (MAO) derived MgO coated Mg alloy improved the survival of MG63 cells,[13] and electrodeposited F-doped hydroxyapatite (F-HA) coated Mg alloy enhanced the proliferation of human bone marrow stromal cells (hBMSCs) compared to the bare ones.[14] The phosphating-derived $CaHPO_4$ coated Mg alloy showed the improved adhesion and proliferation of L929 cells, concurrently promoted bone growth by means of up-regulating osteogenesis-related proteins compared to the naked one.[2] Osteoblasts were observed to adhere and spread well on the sprayed polymer and ion implantation-derived Al_2O_3 coated Mg alloys, and simultaneously

higher volumes of new bone were visible without fibrous capsule around the coated implants compared to the bare ones.[3,15] Chemical deposited HA coated Mg remarkably enhanced adhesion, proliferation and alkaline phosphatase (ALP) activity of MG-63 cells, concurrently new bone formation and bone-to-implant contact compared to the bare one.[16] Although the current studies to some extent demonstrated the response of osteogenetic cells, such as MSCs and osteoblasts, to the coated Mg alloys, the involved are confined to the adhesion and proliferation within a short culture time or single marker denoted differentiation, lack of the detailed investigation of osteogenetic behavior of the cells. Actually, osseointegration of an implant comprised three phases: recruitment of osteogenic cells to the implant surface, differentiation and extracellular matrix (ECM) mineralization of the cells to form new bone on the surface, and peri-implant bone remolding,[17,18] implying the necessity for Mg-based implants to clarify their effect on the differentiation and ECM mineralization of osteogenetic cells. Furthermore, the current *in vivo* implantation studies mainly focused on the amounts of the newly formed bone around the Mg alloys with [2,3,15,16] and without [19] various coatings, and the integration at implant/bone interface was roughly identified by the formation of fibrous capsule or not. However, the interfacial structure and bond mechanism of new bone to Mg-based implants with various coatings were rarely clarified.

Enhanced bone-implant interaction, i.e. promoted amounts of newly formed bone around an implant and improved bone-implant bonding stability, is critical to achieve early bone-implant fixation,[19,20] which in turn depends on the surface chemistry and

topography of an implant. Studies on chemistry drew an enhanced role of HA in promoting cell functions including adhesion, proliferation, differentiation and ECM mineralization, and new bone formation compared to polymers, MgO and other inorganics.[9,11] It is also revealed that narrow interrod spaced Sr-HA nanorods patterned 3-dimensional (3D) topography greatly enhanced osteoblast functions compared to Sr-HA nanogranulated 2D one on Ti.[21,22] Recently, we fabricated a novel coating on Mg using MAO and hydrothermal treatment (HT) for 24 h (termed as HT24h), which comprised HA nanorods with interrod spacing of 63.9 ± 9.0 nm as an outer layer and pores-sealed MgO as an inner layer.[23] The coating provided more effective protection of Mg from corrosion compared to the current methods derived coatings, retaining it coated Mg sufficient mechanical integrity even after 90 days of immersion in physiological saline.[23] Moreover, it greatly enhanced the adhesion and proliferation of hFOB1.19 cells within 5 days compared to MAO-formed porous MgO coating (termed as MAO_0) and short-term HT derived $Mg(OH)_2$-sealing-pores contained MgO coating (termed as HT2h).[23] Herein, we focus our concerns on the role of HT24h-, HT2h- and MAO_0-coated Mg in the regulation of differentiation and ECM mineralization of hFOB1.19 cells in a long period of 3~14 days. Moreover, the osteogenesis of the coated Mg as well as the bone-implant interfacial structure and stability were evaluated in rabbit femora for 8 weeks of implantation, to clarify the correlation between the coatings mediated osteoblast functions and osteogenesis, and the bone-bonding mechanism to the coated Mg.

2. Materials and methods

2.1. Micro-arc oxidation and hydrothermal treatment

To form MAO_0 coatings on Mg, as described previously,[23] commercially pure Mg discs (ϕ 14×4 mm) and pillars (ϕ 2.5×10 mm) were employed as anodes and treated using a pulse power supply in an aqueous electrolyte containing 0.0135 M $Ca(OH)_2$, 0.125 M NaOH, and 0.02 M β-glycerophosphate disodium (β-GP) at an applied voltage of 450 V, a pulse frequency of 100 Hz, and a duty ratio of 26% for 10 min. The resultant MAO_0-coated Mg discs and pillars were then mounted in a Teflon-lined autoclave. 7.8 mL of aqueous solution containing 0.1 M $C_{10}H_{12}CaN_2Na_2O_8$ (Ca-EDTA) and 0.5 M NaOH was added into the autoclave, and the MAO_0-coated Mg were immersed in the solution to undergo HT at 90 ℃ for 2 and 24 h, drawing HT2h and HT24h, respectively. The morphologies and elements contents of the coatings were examined by field-emission scanning electron microscopy (FE-SEM; JEOL JSM-6700F, Japan) equipped with energy-dispersive X-ray spectrometry (EDX).

2.2. Cell proliferation assessment and morphology observation

Human fetal osteoblast cell line, hFOB1.19, was purchased from the Institute of Biochemistry and Cell Biology of Chinese Academy of Sciences (Shanghai, China). The cells were inoculated into complete culture medium (CCM), which comprised Dulbecco's modified Eagle medium (DMEM) supplemented with 10% fetal bovine serum, 0.3 mg/mL Geneticine418 (Sigma, U.S.A.), 0.5 mM sodium pyruvate (Sigma, U.S.A.) and 1.2 mg/L Na_2CO_3, and incubated in a humidified atmosphere incubator

with 5% CO_2 and 95% air at 37 ℃.

The MAO_0-, HT2h- and HT24h-coated Mg discs were sealed with silastic exposing only one side, and placed centrally in 24-well plates with well diameters of 15 mm. hFOB1.19 cells were seeded on the discs with a density of 8×10^4 cells/well and incubated for 3, 7, and 14 days, and the CCM was refreshed every day. At the end of each time period, the CCM was removed from each well, and the samples were washed three times with phosphate buffered saline (PBS; Sigma, U.S.A.) and then transferred to new 24-well plates. To eliminate Mg^{2+} effect on MTT solution, the cells adhered to the samples were digested using 0.5 mL 0.25% trypsin (Sigma, U.S.A.) at 37 ℃ for 10 min, whereupon 0.5 mL of CCM was added to halt digestion and consequently, cell suspensions were obtained. The cell suspensions were quickly centrifuged and resuspended in 250 μL fresh CCM, and then, the cells were reseeded in new 48-well plates and incubated for 24 h to allow the cells to fully attach for MTT assays. Following removal of CCM from each well and subsequent washing three times with PBS, 15 μL of MTT (Sigma, U.S.A.) solution (5 mg/mL MTT in PBS) was added into 250 μL of CCM and cultured for 4 h. The medium was subsequently removed and 100 μL of dimethyl sulfoxide (DMSO; Sigma, U.S.A.) was added to each well and oscillated for 10 min. The resulting DMSO solution was transferred to new 96-well plates and the absorbance was measured at 490 nm. Four specimens from each group were tested, and each test was repeated four times (n=4).

After 3 and 14 days of culture, the cell-adhered samples were washed three times with PBS and fixed with 2.5% glutaraldehyde for 1 h at 4 ℃. The cell-fixed samples

were then dehydrated in ethanol, followed by vacuum drying. After coating gold, the samples were observed under FE-SEM for cell morphologies. The elements contents of the cell-adhered coatings were detected by EDX.

2.3. Osteogenesis-related gene expressions

The total RNA was isolated using the TRIzol reagent (Gibco, U.S.A.). A total of 1 μg of RNA from the cells on each sample was reversed transcribed into complementary DNA using a PrimeScrip RT reagent kit (TaKaRa, Japan). Expressions of osteogenesis-related genes, including runt-related transcription factor 2 (Runx2), osterix, ALP, osteopontin (OPN), osteocalcin (OCN) and collagen I (Col-I), were quantified using a real-time polymerase chain reaction (RT-PCR) detection system (Bio-Rad iQ5 Multicolor) with SYBR® Premix Ex™TaqII (TaKaRa, Japan). Data analysis was carried out using iQ5 Optical System (Bio-Rad, U.S.A.) with software version 2.0. The housekeeping gene, glyceraldehyde-3-phosphate dehydrogenase (GAPDH), was used as an endogenous reference gene to normalize calculation through the comparative Ct value method. The sequences of the specific primers sets were listed as follows: Runx2 (5'-CGACAGCCCCAACTTCC-3' and 5'-TCTTGCCTCGTCCACTCC-3', 60 ℃); osterix (5'-TCCTGCGACTGCCCTAAT-3' and 5'-AGCCTTGCCATACACCTTG-3', 60 ℃); ALP (5'-GGTGGAAGGAGGCAGAAT-3' and 5'-GGGAATGGTCCGCAGTG-3', 60 ℃); OPN (5'-TCGCAGACCTGACATCC-3' and 5'-ACCATTCAACTCCTCGCT-3', 60 ℃); OCN (5'-CCTCACACTCCTCGCCC-3' and 5'-CACTACCTCGCTGCCCTC-3', 58 ℃); Col-I (5'-AAGGTGTTGTGCGATGAC-3' and 5'-GCTGGGGAGCAAAGTT-3', 60 ℃); GAPDH (5'-GAAGGTGAAGGTCGGAGT-3' and

5'-TGGAAGATGGTGATGGG-3', 60 ℃).

2.4. Intracellular ALP activity, specific proteins and Col-I contents as well as intracellular Ca^{2+} and Mg^{2+} concentrations

After 3, 7 and 14 days of culture, the cells seeded samples were washed three times with PBS, and transferred to new cell culture plates, then lysed in 0.1 vol.% Triton X-100 through five standard freeze-thaw cycles and shaken for 10 min. Employing the respective human ELISA kits (Cusabio, U.S.A.) and recording spectrophotometrically the optical absorbance at 450 nm, the intracellular ALP activity, contents of OPN, OCN and Col-I proteins of osteoblasts on the samples were drawn from a standard curve of absorbance vs. known standards of corresponding proteins run in parallel with the tested samples. The results were normalized to the intracellular total protein content. Intracellular Ca^{2+} and Mg^{2+} concentrations were determined using respective calcium and magnesium assay kits (Biovision, U.S.A.) according to the manufacturer's instruction. The absorbance were measured at 450 nm and the intracellular Ca^{2+} and Mg^{2+} concentrations were calculated using the standard provided in the kits. Both the results were normalized to cell numbers. Four samples for each group were tested, and each test was repeated four times (n=4).

2.5. Collagen secretion of osteoblast and ECM mineralization

Collagen secretion by osteoblasts on the samples was quantified by Sirius Red staining as follows. After 3, 7 and 14 days of culture, the cells seeded samples were fixed in 4% paraformaldehyde. The samples were stained for collagen secretion in a saturated picric acid solution containing 0.1% Sirius Red (Sigma, U.S.A.) for 18 h.

After washing with distilled water until no color presented in the water, images of the collagen secreted by osteoblasts on the samples for 7 days were taken. For quantitative analysis, the stain on the samples that osteoblasts were cultured for 3, 7 and 14 days was eluted in 0.5 mL destain solution (0.2 M NaOH/methanol 1:1), then the optical density at 540 nm was measured using a spectrophotometer.

ECM mineralization of osteoblasts was analyzed using Alizarin Red staining. The samples, cultured cells for 3, 7 and 14 days, were fixed in 75% ethanol for 1 h, and subsequently stained with 2% Alizarin Red (Sigma, U.S.A.) solution for 10 min. Afterwards, the samples were washed with distilled water until no color appearing in the distilled water. The images of ECM mineralization were taken at day 14 of culture. For quantitative analysis, the stain on the samples that osteoblasts were cultured for 3, 7 and 14 days was dissolved in 10 mM sodium phosphate aqueous solution containing cetylpyridinum chloride with a volume concentration of 10%, and the absorbance values were measured at 620 nm.

2.6. Immersion tests of the coated Mg discs in serum-free culture medium

Immersion tests of the coated Mg discs were carried out at 37 ℃. All the samples were sealed with silastic exposing only one side and individually soaked in capsules containing 5 mL serum-free cell culture medium for 14 days. The H_2 release from each sample was monitored every two days, together with the pH value of the medium immersing each sample. All tested values were averaged from three specimens for each group at each immersion time point.

2.7. Ionic concentrations of CCM immering coated Mg discs seeded with and

without osteoblasts

The MAO_0-, HT2h- and HT24h-coated Mg discs were sealed with silastic exposing only one side, and placed centrally in 12-well plates. For the measurements of Mg^{2+} and Ca^{2+} released by the coated Mg discs with osteoblasts, the cells suspended in 5 mL CCM were seeded on the samples at a density of 4.4×10^4 cells cm^{-2}; for the measurements of Mg^{2+} and Ca^{2+} released by the coated Mg discs without osteoblasts, 5 mL CCM without cells was injected into the wells to immerse samples. Then they were incubated in a humidified atmosphere incubator with 5% CO_2 and 95% air at 37 ℃. After 1 day of incubation, the CCM from the wells were collected and clarified by centrifugation for 20 min at 1500 rpm at 4 ℃. The supernatants were mixed with 0.5% HNO_3 (supernatant/HNO_3 ratio 1:2) and the concentrations of Mg^{2+} and Ca^{2+} were quantified by inductively coupled plasma atomic emission spectrometry (ICP-AES; PerkinElmer, Optima 3000Dv, U.S.A.) and corrected for subtraction of the initial concentrations of Mg^{2+} and Ca^{2+} in CCM. All tested values were averaged from three specimens for each group at each immersion time point.

2.8. Animal experiment

All the animal experiments were conducted according to the ISO 10993-2: 1992 animal welfare requirements and approved by the Institutional Animal Care and Use Committee of Xi'an Jiaotong University. Nine adult male New Zealand rabbits weighing 2.0~2.5 kg were used, as employed by Liu [24] and Chang [25] in their animal tests. They were kept individually in clean plastic cages with standard bedding, water and standard diets. Before the surgery, all the rabbits were subjected to the clinical

checks. Then each rabbit was anesthetized by an intramuscular injection of 2.5 wt.% pentobarbital sodium solution. The chosen operation site was femur diaphysis, and each rabbit was implanted with one kind of the coated Mg pillar. Two holes (ϕ 2.5 mm) were respectively drilled on right and left femur shafts of each rabbit using a disinfected hand-operated drill, during which the operation sites were cooled with physiological saline (0.9 wt.%). Then two coated Mg pillars were inserted into the pre-drilled holes. The muscle layers, subcutaneous tissue and skin were sewed up subsequently. Postoperatively, the rabbits were allowed to move freely in their cages without external support. All the rabbits received a subcutaneous injection of brizolina (antibiotics) for three days after surgery.

After eight weeks of implantation, the rabbits were sacrificed by intraperitoneal injection of an overdose of pentobarbitone sodium. Immediately, the femora containing the implants from the rabbits were harvested. Nine of the femora (n=3 for each group) were fixed in neutral buffered formalin, dehydrated by ascending concentrations of ethanol, and finally embedded in polymethyl methacrylate (PMMA). For histological examination, the embedded specimens was cut into 150 μm thick sections using a saw microtome (Leitz1600, Hamburg, Germany), ground and polished to a final thickness of about 20~30 μm, consequently the sections were stained using Van Gieson's picric-fuchsine. Digital microscopic images were captured on a microscopy (Olympus IX 71, Olympus, Japan) and analyzed using Image-ProPlus software. The percentage of bone-implant contact was assessed on 3 sections on each implant as described in details elsewhere.[24] In addition, the

microstructures of the implant/bone interfaces were observed by FE-SEM with EDX.

According to the previous work,[25] the push-out tests were carried out on other nine femora containing implants (n=3 for each group) to assess the strength of bone-implant integration. Each of the femora containing implants was mounted on a test fixture which was allowed for an accurate alignment of the sample with strictly perpendicular axial load transfer. Subsequently, the testing machine pushed the implant vertically out at a cross-head speed of 1 mm/min. The load-displacement curve for each sample was recorded and the push-out force can be drawn from the curve. After the tests, the obtained coated Mg pillars were rinsed with flowing deionized water and dried at room temperature. After coating gold, the surface morphologies and elements components of the pushed-out surfaces on the side of coated pillars were examined by FE-SEM with EDX to clarify the push-out derived failure modes. Five FE-SEM images were captured for each group to evaluate area percentage of every failure mode on the disrupted surfaces of the pillars.

2.9. Statistical analysis

The data were analyzed using SPSS 16.0 software (SPSS, U.S.A.). A one-way ANOVA followed by a Student-Newman-Keuls post hoc test was used to determine the level of significance, as employed by Liu [24] and Chang [25] in their animal tests. $p < 0.05$ was considered to be significant and $p < 0.01$ was considered to be highly significant.

3. Results and discussion

3.1. Surface morphologies of MAO_0, HT2h and HT24h coatings

As described in our work,[23] MAO_0 was composed of porous MgO; HT2h consisted of MgO containing pores sealed with $Mg(OH)_2$ nanoplates as an inner layer and a thin coverage of $Mg(OH)_2$ nanoplates as an outer layer; HT24h comprised an inner layer of MgO containing pores sealed with HA nanorods and $Mg(OH)_2$ nanoplates and an outer layer of HA nanorods, in which the roots of the HA nanorods were embedded in the MgO matrix and the $Mg(OH)_2$ nanoplates were among the HA nanorods. Moreover, HT24h adhered firmly to Mg, and retained relatively high bonding integrity even after 90 days of immersion in physiological saline.[23] The FE-SEM surface morphologies of the coatings are shown in Figs. 1a-c, and the architecture of HT24h-coated Mg is schematically shown in Fig. 1d. Notably, the HA nanorods on HT24h are about 93.8±7.1 nm in diameter and 64.6±6.6 nm in interrod spacing, consistent with the values reported previously.[23] It has been reported that during bone resorption by activated osteoclasts at bone remodeling sites, ruffled membrane of osteoclasts with invaginated surface penetrates the bone matrix to a depth of approximately 1 μm, achieving the dissolution of inorganic matrix and enzymatic degradation of organic components. Consequently, the bone exposed by osteoclastic resorption demonstrated an apparently demineralized, microporous collagenous surface, on which the exposed collagen revealed 3D nanofibrous topography aligned either perpendicular or quasi-vertical to the resorption surface.[18] Herein, the surface morphological feature of HT24h is quite similar to the osteoclast-created 3D nanotopography comprising demineralized collagen of bone

matrix at bone remodeling sites, into which cement line matrix can be deposited to form a bonding of new bone to old bone.[18]

3.2 Cell proliferation on MAO_0-, HT2h- and HT24h-coated Mg discs

As presented previously, the counting assay based on fluorescent observations of stained hFOB1.19 cells revealed little live cells on bare Mg but pronounced live cells on the coated Mg at 1~5 days, and the coated Mg showed significant increase in the number of live cells with incubation time, consistent with the variation trend assessed by MTT.[23] Owing to the connection of hFOB1.19 cells on the coated Mg at days 7 and 14, it is difficult to count and thereby cell growth on the coated Mg within 3~14 days was herein assessed by MTT, as shown in Fig. 2a. Although MTT assay actually reflects mitochondrial activity of cells, the consistence between MTT and counting assays within 1~5 days [23] indicate that MTT assay can indirectly assesses the number of live cells. The mitochondrial activities of cells on the coated Mg increased with incubation from 3 to 14 days, indirectly suggesting that the cells proliferated after 3 days but faster on HT24h-coated Mg than HT2h-coated Mg and much faster than MAO_0-coated Mg (Fig. 2a). Notably, although the mitochondrial activities of all the cells cultured on HT24h-coated Mg still increased after 7 days of incubation, the rising rate slowed down compared to that at initial incubation period, which was attributed to a reduced tendency for cellular proliferation by already started osteogenic differentiation.[26] Cell proliferation is marked by the induction of ECM composed of collagen and noncollagenous proteins.[23] Whereupon, analyses of the collagen secreted by cells on the coated Mg after 3~14 days of incubation were undertaken, as shown in

Figs. 2b and 2c. It is clear that osteoblasts were able to form ECM on all the coated Mg within 3 days, however, the collagen secretion marked cell proliferation was significantly enhanced on HT24h-coated Mg compared to MAO_0- and HT2h-coated Mg.

3.3. Cell differentiation on MAO_0-, HT2h- and HT24h-coated Mg discs

Differentiation of osteoblasts can be divided into three main periods: ECM synthesis, maturation and mineralization.[27,28] Here the osteoblast differentiation on the coated Mg was identified by examining the variations of intracellular osteogenesis-related markers, including Runx2, osterix, ALP, OPN, OCN and Col-I, at both levels of gene and protein or activity with incubation time. Expressions of osteogenesis-related genes on the coated Mg at 3, 7 and 14 days are shown in Fig. 3. For Runx2, osterix, OCN, OPN and Col-I, the coated Mg are observed to up-regulate their mRNA levels with incubation from 3 to 14 days; at each time, their mRNA levels on the coated Mg follow the order: HT24h>HT2h>MAO_0. Regarding to ALP, its gene expression keeps on up-regulating on MAO_0- and HT2h-coated Mg with incubation from 3 to 14 days, however, reveals a peak level at day 7 on HT24h-coated Mg. At levels of ALP activity and protein contents of OPN, OCN and Col-I on the coated Mg (Fig. S1), their variation trend with incubation time is similar to that of the corresponding gene expressions. These results indicate that HT24h-coated Mg greatly promotes the synthesis of intracellular osteogenesis-related markers compared to MAO_0- and HT2h-coated Mg.

Fig. 4a shows the Alizarin Red staining assays of ECM mineralization on the

coated Mg after cell incubation for 3, 7 and 14 days, revealing that HT24h-coated Mg significantly promotes ECM mineralization compared to HT2h-coated Mg, and this promoting efficacy is more pronounced compared to MAO_0-coated Mg. Figs. 4b and 4c show the FE-SEM images of cells on the coated Mg at days 3 and 14, and the EDX-detected Ca and P contents of cells are exhibited in Table 1. Compared to the relatively smooth surfaces of cells on all the coated Mg at day 3, a few of mineral particles appeared on the surfaces of cells at day 14. Notably, the increments in Ca and P contents (at.%) detected on cells' surfaces between days 14 and 3 are 1.5 and 2.4 for MAO_0-coated Mg, 3.4 and 3.7 for HT2h-coated Mg, and 4.4 and 5.9 for HT24h-coated Mg, respectively, further indicating an enhanced ECM mineralization on HT24h-coated Mg.

Runx2 is a transcription factor for early osteoblast differentiation,[29] while osterix is a zinc finger transcription factor to induce differentiation of osteoblast to a mature phenotype.[30] ALP is a key marker of osteoblast differentiation with peak levels of gene and activity during osteoblast maturation, and the levels then decrease at the onset of ECM mineralization.[28] OPN is a middle-stage marker of osteogenic differentiation associated with the onset of ECM mineralization,[31] and OCN is a late-stage marker of osteoblast differentiation.[32] Here, the Runx2, osterix and ALP mRNA and ALP activity were enhanced on HT24h-coated Mg compared to MAO_0- and HT2h-coated Mg at days 3 and 7, indicating that HT24h-coated Mg accelerated differentiation by promoting cell maturation; moreover, the HT24h-caused decrease in ALP following day 7 further suggests that the cell differentiation progressed into the

period of ECM mineralization at time as earlier as day 7. In the ordered sequence of events occurring during osteoblast differentiation, the increase in ALP activity is followed by the increased synthesis of Col-I and then the deposition of noncollagenous ECM proteins such as OPN and OCN to form bone.[28] Our results at both levels of gene and protein revealed that the synthesis of intracellular Col-I, OPN and OCN was greatly enhanced on HT24h-coated Mg, which would lead to more secretion of these proteins into ECM and thereby accelerated ECM mineralization on HT24h-coated Mg. Overall, HT24h-coated Mg accelerated osteoblast differentiation, not only promoting the cells to a mature phenotype but also expediting ECM mineralization at an earlier time compared to MAO_0- and HT2h-coated Mg.

The contact of Mg with an aqueous solution could result in Mg degradation to release Mg^{2+} and H_2, and alkalization of the solution.[5] As an anchorage-survival cell, osteoblasts respond to the coated Mg depending on two factors: the surface features of a material to which the cells adhere and the medium in which the cells are located. Previous studies on chemistry have described the enhanced role of HA in promoting cell functions compared to MgO and $Mg(OH)_2$.[11] In addition, surface topographies of materials play a critical role in the regulation of cell proliferation and differentiation. In the case of microroughened surfaces derived by sandblasting and/or acid etching, an inverted correlation between cell proliferation and differentiation has been revealed. For instance, microroughened surfaces promoted osteoblast differentiation and bone maturation, whereas reduced osteoblast proliferation and accordingly resulted in smaller bone mass around them compared with relatively smooth surfaces.[33-36]

Different from the microroughened surfaces, however, hierarchical micro-nano-hybrid topographies, such as a micro/nano-textured surface with titania nanotubes derived by anodization of acid-etched titanium [37] and a micropit-nanonodule hybrid topography fabricated by nanonodule self-assembly on acid-etched titanium,[38] have been reported to simultaneously promote osteoblast proliferation and differentiation. Moreover, our works on topography also revealed that 3D Sr-HA nanorods patterned Ti with interrod spacing < 70 nm could accelerate the proliferation, differentiation and ECM mineralization of osteoblasts compared to 2D Sr-HA nanogranulats.[21,22] In our present study, HT24h comprises an inner layer of MgO containing micron-scaled pores sealed with HA nanorods and $Mg(OH)_2$ nanoplates and an outer layer of HA nanorods with interrod spacing of 64.6±6.6 nm, constructing a hierarchical micro/nano-structured topography (Figs. 1c and d). Hence, the HT24h-expedited osteoblast proliferation, differentiation and ECM mineralization partially ascribed to the hierarchical micro/nano feature of the coating. To clarify the cells located environment, the H_2 release and pH values of the serum-free culture media immersing the coated Mg as a function of immersion time were measured, moreover, due to daily refreshment of CCM, Ca^{2+} and Mg^{2+} concentrations of the coated Mg seeded with and without osteoblasts immersed CCM were also tested after 1 day immersion, as shown in Fig. 5. Following immersion for the same duration, the H_2 release (Fig. 5a) and alkalization of the coated Mg immersed media (Fig. 5b) are lightened in the order of HT24h<HT2h<MAO_0. It has been reported that H_2-enriched DMEM can be well tolerated by pre-osteoblasts with more than 90% viability and the presence of

moderate amount of H_2 in the medium gives rise to a significantly higher ALP activity.[3] However, excessive H_2 release resulting from rapid degradation of Mg-based implants is a major concern,[7] the accumulation of subcutaneous H_2 gas can lead to cell damage and inhibit the healing process of fractured bone.[39] It has been reported that subcutaneous gas bubble would form when the evolution rate of H_2 exceeds 0.068 mL/cm^2/day.[40] Regarding to pH value, Shen et al. found that proliferation and ALP activity of osteoblast were significantly enhanced with increasing pH up to 8-8.5.[41] It has to be pointed out that the alkalization caused by the corrosion of Mg can result in a fast increase in pH value of SBF to 10.5, which is undesirable for the adhesion, growth and proliferation of cells.[2,42] In our present work, H_2 release rate of HT24h-coated Mg was about 0.065 mL/cm^2/day (Fig. 5a), lower than the tolerant evolution rate, indicating that gas accumulation would not occur after implantation to damage the surrounding tissue and inhibit bone formation. Moreover, after immersion for 14 days, the pH value of the serum-free culture medium immersing HT24h-coated Mg steadily increased to about 8.5 (Fig. 5b). Therefore, the HT24h-coated Mg derived lightened H_2 evolution and alkalization, which resulted from the enhanced protection of the underling Mg from corrosion by HT24h than MAO_0 and HT2h,[23] could provide a moderate environment beneficial to osteoblast survival and differentiation.

Most importantly, the degradation of the coated Mg also altered the Ca^{2+} and Mg^{2+} concentrations of surrounding CCM (Figs. 5c-f). After immersion for 1 day, the Ca^{2+} and Mg^{2+} concentrations of surrounding CCM released by the coated Mg seeded

with and without osteoblasts have no significant differences. Noticeably, regardless of cell seeding or not, HT24h-coated Mg resulted in lower Ca^{2+} and Mg^{2+} concentrations of surrounding medium compared to HT2h-coated Mg, while MAO_0-coated Mg released the highest Ca^{2+} and Mg^{2+} concentrations, owing to the inhibited degradation of Mg and MgO by the overlying HA and $Mg(OH)_2$ in HT24h. It suggests that HT24h-coated Mg could result in lower extracellular Ca^{2+} and Mg^{2+} concentrations (denoted as $[Ca^{2+}]_e$ and $[Mg^{2+}]_e$, respectively) compared to HT2h- and MAO_0-coated Mg during cell culture. As known, $[Ca^{2+}]_e$ and $[Mg^{2+}]_e$ can mediate cell behavior via regulating intracellular Ca^{2+} and Mg^{2+} concentrations (denoted as $[Ca^{2+}]_i$ and $[Mg^{2+}]_i$, respectively).[21,43-45] To clarify the effect, the $[Ca^{2+}]_i$ and $[Mg^{2+}]_i$ of cells incubated on the coated Mg for 3, 7 and 14 days were examined, as show in Fig. 6. At each incubation point, $[Ca^{2+}]_i$ was remarkably up-regulated by HT24h-coated Mg relative to MAO_0- and HT2h-coated Mg, revealing a contrary regulation trend to $[Ca^{2+}]_e$ (Figs. 5c and 5d). However, $[Mg^{2+}]_i$ was greatly down-regulated by HT24h-coated Mg relative to MAO_0- and HT2h-coated Mg, revealing a similar regulation trend to $[Mg^{2+}]_e$ (Figs. 5e and 5f). Given that the increased $[Ca^{2+}]_e$ would lead to an increase in $[Ca^{2+}]_i$ through voltage gate Ca^{2+} channels (VDCC) of cells.[46] While the increased $[Mg^{2+}]_e$ would not only increase the $[Mg^{2+}]_i$,[47,48] but also decrease the $[Ca^{2+}]_i$.[49] This is related to that Mg^{2+} channels of cells can be activated by the additional extracellular Mg^{2+} and allow them influx.[48] However, Mg^{2+} is an antagonist to Ca^{2+} and both of them compete to employ the same transporters, for example, transient receptor potential melastin 7 (TRPM7) channel.[44] The influent Mg^{2+} would block TRPM7

channel and higher $[Mg^{2+}]_i$ could also shut down VDCC channel, inhibiting Ca^{2+} transportation from outside to inside of the cells and leading to the reduction of $[Ca^{2+}]_i$.[44,45,50] Herein, the significant up-regulation of $[Ca^{2+}]_i$ even in the case of lower $[Ca^{2+}]_e$ and down-regulation of $[Mg^{2+}]_i$ for cells on HT24h-coated Mg compared to the other groups are attributed to the lower Mg^{2+} released from the former than the later (Figs. 5e and 5f). Besides the effect of $[Ca^{2+}]_e$ and $[Mg^{2+}]_e$, the surface topographies of the coatings can also regulate $[Ca^{2+}]_i$. We have demonstrated that 3D Sr-HA nanorods patterned Ti with < 70 nm interrod spacing independently up-regulated $[Ca^{2+}]_i$ compared to 2D Sr-HA.[22] Thus the narrow interrod spaced HA nanorods patterned HT24h exerts a positive effect on the elevated $[Ca^{2+}]_i$.

$[Ca^{2+}]_i$ and $[Mg^{2+}]_i$ play a key role in the regulation of cell behavior. The up-regulation of $[Ca^{2+}]_i$ induces osteoblast proliferation by activation of CaMKII and c-fos expressions, and promotes differentiation by activation of fra-2 expression.[33] Moreover, proliferation and osteoblastic differentiation of MSCs can be enhanced with increasing $[Ca^{2+}]_i$.[30] In contrast, $[Mg^{2+}]_i$ shows a dose-dependent effect on regulating osteoblast functions. Deficient $[Mg^{2+}]_i$ was reported to decrease osteoblast activity and impair bone-remolding;[44] whereas overdose $[Mg^{2+}]_i$ would compete with $[Ca^{2+}]_i$ for common intracellular binding sites and suppress spontaneous release of adenosine triphosphate, retarding ECM mineralization of hBMSCs.[45,48] To maintain normal cell functions, $[Mg^{2+}]_e$ should keep below a threshold value of 1.3 mM, especially the differentiation and mineralization of hBMSCs was reported to enhance when it was lower than 1.05 mM.[45] As calculated according to Fig. 5f, the Mg^{2+}

concentrations of the CCM surrounding cells on MAO_0-, HT2h- and HT24h-coated Mg, at the end of the daily refreshment, are about 1.56±0.09, 1.23±0.05 and 0.94±0.06 mM, respectively. Of which the Mg^{2+} concentration of the CCM surrounding HT24h-coated Mg is lower but that of MAO_0-coated Mg is higher than the threshold $[Mg^{2+}]_e$ of 1.3 mM. Therefore, the expedited differentiation and ECM mineralization by HT24h-coated Mg are mainly attributed to the up-regulated $[Ca^{2+}]_i$ and down-regulated $[Mg^{2+}]_i$ relative to MAO_0- and HT2h-coated Mg, in parallel to the attribution of the lightened H_2 evolution and alkalization.

3.4. In vivo osseointegration of the coated Mg pillars

Following implantation in rabbit femora for 8 weeks, the rectangle-marked region on each of the coated Mg pillars (Fig. 7a), which is adjacent to the cortico-cancellous bone but in the bone marrow cavity, was imaged to evaluate new bone formation. With this region, what evaluated is contact rather than distance osteogenesis. The histological stained images (Fig. 7b) show new bone to be formed on all the coated pillars without intervening fibrous layers. However, the new bone thickness and bone-implant contact (Fig. 7c) are quite different, showing the highest values on HT24h-coated pillar and the lowest values on MAO_0-coated pillar. This result is further supported by FE-SEM images (Fig. 7d), in which the components of new bone, coating and underlying Mg on each bone-implant cross-section was clarified by the EDX-detected elemental profiles. Noticeably even at high magnification, HT24h still revealed a tight contact with new bone at most area of the coating/bone interface, while a large area of gap presented between MAO_0 and new

bone. In spite of the case, the MAO_0-coated pillar still exhibited an improved osteogenesis than bare Mg pillar in terms of the new bone thickness and bone-implant contact (Fig. S2). Ascribed to the difference in percentage of bone-implant contact, the bone/implant interfacial strength of the coatings coated pillars, as measured by push-out test, followed the rank of HT24h>HT2h>MAO_0 (Fig. 7e).

The push-out disrupted surfaces on the sides of the coated Mg pillars were examined by FE-SEM and EDX. For HT24h-coated pillar, as representatively shown in Fig. 8, three kinds of failure modes can be observed on the disrupted surface from Fig. 8a imaged region 1. One is within the newly formed bone (site A in Fig. 8a), as verified by point 1 detected high Ca and P contents. The other is at bone/coating interface (site B in Fig. 8a), as identified by the emergence of nanorods at magnification of the site (Fig. 8b) and the points 2 and 3 detected Ca and P contents similar to those of the point σ detected HA nanorods (Fig. 8e). The third appears at corrosion pits (site C in Fig. 8a), as supported by the fact that high contents of Mg and O but almost no Ca and P could be detected at magnification of the pit (point 4 in Fig. 8c). The area percentage of the three kinds of failure modes were counted as shown in Fig. 8f, indicating that the disruption within the peri-implant bone is a predominant failure mode for HT24h-coated pillar. Although the disruption at bone/coating interface, as demonstrated in Fig. 8b, is rarely presented on the whole surface, such image that shows a Ca, P and C richened thin layer underlying the new bone but overlying the HA nanorods, does provide the insights of how the newly formed bone bind to the coating. More detailed overlap between the Ca, P and C richened matrix

and the underlying HA nanorods can be observed from Fig. 8d imaged region 2. It is clearly revealed that the matrix firstly deposited to wrap each of the HA nanorods, then filled the interrod space and finally formed a layer to overlay the HA nanorods. The Fig. 8d depicted wrappage surrounding the HA nanorods is different in morphology from the HA-induced apatite in simulated body fluid as early as 12 h (Fig. S3), suggesting that the former was not induced by HA. However, this Ca, P and C richened layer is similar in chemistry to the cement line matrix between new and old bone during bone-remodeling, which has been proved to be formed by the mineralization of osteoblasts-secreted noncollagenous proteins such as bone sialoprotein and OPN.[18,51] Whereafter, osteoblasts secreted collagen overlying the cement line matrix and the collagen fibers were further mineralized to form bony matrix.[18,51] It is reasonable to deduce that the Ca, P and C richened layer overlying the HA nanorods, in the present work, could act as the cement line matrix to form mechanical interdigitation [18,51] or chemical bonding [20] with the HA nanorods, which can significantly enhance the integration strength of the HT24h-coated pillar to bone. The enhanced *in vivo* osteogenesis and osseointegration of HT24h-coated pillar is well in line with its enhanced *in vitro* effect on osteoblast functions.

Different from HT24h-coated pillar, when pushed-out, HT2h-coated pillar was observed to disrupt predominantly within the coating but near its surface, besides at corrosion pits and the coating/Mg interface (Fig. S4); whereas MAO_0-coated pillar failed mainly at the coating/Mg interface, besides within the coating but far from its surface, and at corrosion pits (Fig. S5), as counted in Fig. 8f. This is related to the

pores pronounced in HT2h and more pronounced in MAO_0 compared to HT24h, which results in lower barrier ability of the former (especially MAO_0) to corrosive fluid. We have found that after immersion in physiological saline for 90 days, more MgO adjacent to the surface of HT2h converted to $Mg(OH)_2$ while more Mg degradation-derived $Mg(OH)_2$ formed at the MgO/Mg interface in MAO_0-coated Mg.[23] Consequently, MAO_0 and HT2h exhibited a relatively fast drop in scratch-tested bonding strength after immersion, and the scratch-derived failure occurred at the MgO/Mg interface for MAO_0 and the upper $Mg(OH)_2$/MgO interface for HT2h.[23]

4. Conclusions

A bio-inspired coating (HT24h), comprising an outer layer of narrow interrod spaced HA nanorods mimicking the osteoclasts-created 3D nanotopography of bone matrix at remodeling sites and an inner layer of pores-sealed MgO, was fabricated on Mg using MAO and HT. Compared to porous MgO (MAO_0)- and $Mg(OH)_2$-sealing-pores contained MgO (HT2h)-coated Mg, HT24h-coated Mg greatly enhanced osteoblast functions including proliferation, differentiation and ECM mineralization, which ascribed to the lightened H_2 evolution and alkalization of surrounding medium as well as the up-regulated $[Ca^{2+}]_i$ and down-regulated $[Mg^{2+}]_i$. The down-regulated $[Mg^{2+}]_i$ resulted from the lower Mg^{2+} release from HT24h-coated Mg, whereas the up-regulated $[Ca^{2+}]_i$ is related to the lower Mg^{2+} release and the Mg^{2+} blocking effect on the influx of Ca^{2+} to cells, and partially attributed to the

positive effect of the HA nanorods on $[Ca^{2+}]_i$. Owing to the enhanced osteoblast functions, HT24h-coated Mg greatly enhanced osteogenesis, bone-implant contact and push-out force characterized osseointegration and its pushed-out failure occurred predominantly within the peri-implant bone rather than within the coating for HT2h-coated Mg and at the coating/Mg interface for MAO_0-coated Mg.

Associated content

Electronic supplementary information (ESI) available:

ALP activity as well as contents of Col-I, OPN, and OCN proteins in osteoblasts cultured on MAO_0-, HT2h- and HT24h-coated Mg for 3, 7, and 14 days; Histological analysis performed on the cross-section of bare Mg pillar implanted in rabbit femur for 8 weeks and cross-sectional FE-SEM morphology at the interface of new bone and the bare pillar together with the magnified image of the interface, showing an obvious gap; Low-magnification FE-SEM surface morphology of the HT24h-coated Mg disc immersed in SBF for 12 h together with the magnified image; FE-SEM surface image of the pushed-out disrupted surface on HT2h-coated Mg pillar implanted in rabbit femur for 8 weeks, and magnified image; FE-SEM surface image of the pushed-out disrupted surface on MAO_0-coated Mg pillar implanted in rabbit femur for 8 weeks and magnified image.

Acknowledgements

We appreciate the National Program on Key Basic Research Project (973

Program) of China (Grant number 2012CB619103) and National Natural Science Foundation of China (Grant number 51371137, 51071120) for financially supporting this work.

References

1 M. P. Staiger, A. M. Pietak, J. Huadmai and G. Dias, *Biomaterials*, 2006, **27**, 1728-1734.

2 L. P. Xu, F. Pan, G. N. Yu, L. Yang, E. L. Zhang and K. Yang, *Biomaterials*, 2009, **30**, 1512-1523.

3 H. M. Wong, Y. Zhao, V. Tam, S. L. Wu, P. K. Chu, Y. F. Zheng, M. K. T. To, F. K. L. Leung, K. D. K. Luk, K. M. C. Cheung and K. W. K. Yeung, *Biomaterials*, 2013, **34**, 9863-9876.

4 A. F. Cipriano, A. Sallee, R. G. Guan, Z. Y. Zhao, M. Tayoba, J. Sanchez and H. N. Liu, *Acta Biomater.*, 2015, **12**, 298-321.

5 Y. F. Zheng, X. N. Gu and F. Witte, *Mater. Sci. Eng., R.*, 2014, **77**, 1-34.

6 M. Alvarez-Lopez, M. D. Pereda, J. A. del Valle, M. Fernandez-Lorenzo, M. C. Garcia-Alonso, O. A. Ruano and M. L. Escudero, *Acta Biomater.*, 2010, **6**, 1763-1771.

7 B. Zberg, P. J. Uggowitzer and J. F. Loffler, *Nature Mater.*, 2009, **8**, 887-981.

8 J. W. Seong and W. J. Kim, *Acta Biomater.*, 2015, **11**, 531-542.

9 H. Hornberger, S. Virtanen and A. R. Boccaccini, *Acta Biomater.*, 2012, **8**, 2442-2455.

10 T. S. N. S. Narayanan, Il. S. Park and M. H. Lee, *Prog. Mater. Sci.*, 2014, **60**, 1-71.

11 S. Shadanbaz and G. J. Dias, *Acta Biomater.*, 2012, **8**, 20-30.

12 E. L. Zhang, L. P. Xu, G. N. Yu, F. Pan and K. Yang, *J. Biomed. Mater. Res., Part A*, 2009, **90A**, 882-893.

13 X. N. Gu, N. Li, W. R. Zhou, Y. F. Zheng, X. Zhao, Q. Z. Cai and L. Q. Ruan, *Acta Biomater.*, 2011, **7**, 1880-1889.

14 J. N. Li, Y. Song, S. X. Zhang, C. L. Zhao, F. Zhang, X. N. Zhang, L. Cao, Q. M. Fan and T. T. Tang, *Biomaterials*, 2010, **31**, 5782-5788.

15 H. M. Wong, K. W. K. Yeung, K. O. Lam, V. Tama, P. K. Chu, K. D. K. Luk and K. M. C. Cheung, *Biomaterials*, 2010, **31**, 2084-2096.

16 S. M. Kim, J. H. Jo, S. M. Lee, M. H. Kang, H. E. Kim, Y. Estrin, J. H. Lee, J. W. Lee and Y. H. Koh, *J. Biomed. Mater. Res., part A*, 2014, **102A**, 429-441.

17 J. E. Davies, E. Ajami, R. Moineddin and V. C. Mendes, *Biomaterials*, 2013, **34**, 3535-3546.

18 J. E. Davies, *Biomaterials*, 2007, **28**, 5058-5067.

19 C. Castellani, R. A. Lindtner, P. Hausbrandt, E. Tschegg, S. E. Stanzl-Tschegg, G. Zanoni, S. Beck and A. Weinberg, *Acta Biomater.*, 2011, **7**, 432-440.

20 Y-T. Sul, C. Johansson, E. Byon and T. Albrektsson, *Biomaterials*, 2005, **26**, 6720-6730.

21 Y. Han, J. H. Zhou, S. M. Lu and L. Zhang, *Rsc Adv.*, 2013, **3**, 11169-11184.

22 J. H. Zhou, B. Li, S. M. Lu, L. Zhang and Y. Han, *ACS Appl. Mater. Interfaces*, 2013, **5**, 5358-5365.

23 B. Li, Y. Han and K. Qi, *ACS Appl. Mater. Interfaces*, 2014, **6**, 18258-18274.

24 Y. Q. Qiao, W. J. Zhang, P. Tian, F. H. Meng, H. Q. Zhu, X. Q. Jiang, X. Y. Liu and P. K. Chu, *Biomaterials*, 2014, **35**, 6882-6897.

25 C. T. Wu, Z. T. Chen, Q. J. Wu, D. L. Yi, T. Friis, X. B. Zheng, J. Chang, X. Q. Jiang and Y. Xiao, *Biomaterials*, 2015, **71**, 35-47.

26 V. Kishore, W. Bullock, X. B. Sun, W. S. Van Dyk and O. Akkus, *Biomaterials*, 2012, **33**, 2137-2144.

27 B. Setzer, M. Bachle, M. C. Metzger and R. J. Kohal, *Biomaterials*, 2009, **30**, 979-990.

28 O. Tsigkou, J. R. Jones, J. M. Polak and M. M. Stevens, *Biomaterials*, 2009, **30**, 3542-3550.

29 T. Komori, *J. Cell. Biochem.*, 2006, **99**, 1233-1239.

30 K. Nakashima, X. Zhou, G. Kunkel, Z. P. Zhang, J. M. Deng, R. R. Behringer and B. D. Crombrugghe, *Cell*, 2002, **108**, 17-29.

31 A. Dolatshahi-Pirouz, T. Jensen, D. C. Kraft, M. Foss, P. Kingshott, J. L. Hansen, A. N. Larsen, J. Chevallier and F. Besenbacher, *ACS Nano*, 2010, **4**, 2874-2882.

32 V. Viereck, H. Siggelkow, S. Tauber, D. Raddatz, N. Schutze and M. Hufner, *J. Cell. Biochem.*, 2002, **86**, 348-356.

33 H. Aita, N. Hori, M. Takeuchi, T. Suzuki, M. Yamada, M. Anpo and T. Oqawa, *Biomaterials*, 2009, **30**, 1015-1025.

34 T. Ogawa and I. Nishimura, *Int. J. Oral Maxillofac Implants*, 2003, **18**, 200-210.

35 T. Ogawa, C. Sukotjo and I. Nishimura, *J. Prosthodont*, 2002, **11**, 241-247.

36 K. Takeuchi, L. Saruwatari, H. K. Nakamura, J. M. Yang and T. Ogawa, *J. Biomed. Mater. Res., Part A*, 2005, **72A**, 296-305.

37 L. Z. Zhao , S. L. Mei, P. K. Chu, Y. M. Zhang and Z. F. Wu, *Biomaterials*, 2010, **31,** 5072-5082.

38 K. Kubo, N. Tsukimura, F. Iwasa, T. Ueno, L. Saruwatari, H. Aita, W. A. Chiou and T. Ogawa, *Biomaterials*, 2009, **30**, 5319-5329.

39 X. B. Chen, D. R. Nisbet, R. W. Li, P. N. Smith, T. B.Abbott, M. A. Easton, D. H. Zhang and N. Birbilis. *Acta Biomater.*, 2014, **10**, 1463-1474.

40 G. L. Song, *Corros. Sci.*, 2007, **49**, 1696-1701.

41 Y. H. Shen, W. C. Liu, C. Y. Wen, H. B. Pan, T. Wang, B. W. Darvell, W. W. Lu, and W. H. Huang, *J. Mater. Chem.*, 2012, **22**, 8662-8670.

42 G. L. Song and S. Z. Song, *Adv. Eng. Mater.*, 2007, **9**, 298-302.

43 A. M. Barradas, H. A. Fernandes, N. Groen, Y. C. Chai, J. Schrooten, J. van de Peppel, J. P. van Leeuwen, C. A. van Blitterswijk and J. de Boer, *Biomaterials*, 2012, **33**, 3205-3215.

44 M. Leidi, F. Dellera, M. Mariotti and J. A. M. Maier, *Magnesium Res.*, 2011, **24**, 1-6.

45 L. Zhang, C. X. Yang, J. Li, Y. C. Zhu and X. L. Zhang, *Biochem. Bioph. Res. Co.*, 2014, **450**, 1390-1395.

46 M. Zayzafoon, *J. Cell. Biochem.*, 2006, **97**, 56-70.

47 A. Zhang, T. P. O. Cheng, B. T. Altura and B. M. Altura, *Pflug. Arch. Eur. J. Phy.*, 1992, **421**, 391-393.

48 J. L. Wang, F. Witte, T. F. Xi, Y. F. Zheng, K. Yang, Y. S. Yang, D. W. Zhao, J. Meng, Y. D. Li, W. R. Li, K. M. Chan and L. Qin, *Acta Biomater.*, 2015, **21**, 237-249.

49 K. Elizabeth, D'A. Gilbert, H. A. Singer and C. M. Rembold, *J. Clin. Invest.*, 1992, **89**, 1988-1994.

50 H. C. Hartzell and R. E White, *J Gen Physiol.*, 1989, **94**, 745-767.

51 J. E. Davies, V. C. Mendes, J. C.H. Ko and E. Ajami, *Biomaterials*, 2014, **35**, 25-35.

Table of Contents/Abstract Graphic

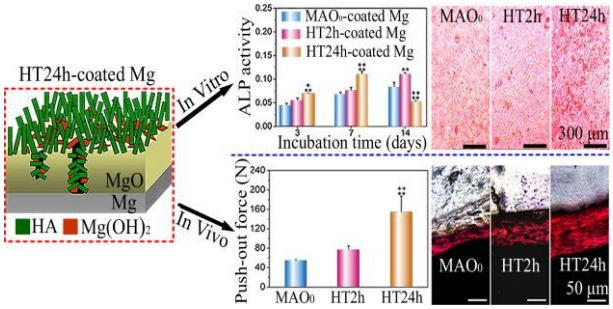

Osteogenetic capability of Mg was significantly enhanced by a bio-inspired hydroxyapatite (HA) nanorods patterned pores-sealed MgO bilayer coating.

Table 1. Element contents detected by EDX in the square-marked on the cells shown in Figs. 4b and c, together with the differences in the element contents of calcium and phosphorus between 3 and 14 days of incubation.

Coatings	Incubation time (days)	Element contents (atom. %)					Difference in the element contents	
		Mg	O	C	Ca	P	ΔCa	ΔP
MAO_0	3	5.9 ± 0.7	35.8 ± 5.0	17.3 ± 2.4	6.4 ± 1.4	10.1 ± 1.0	1.5	2.4
	14	4.8 ± 2.2	33.5 ± 1.9	17.4 ± 0.6	7.9 ± 1.1	12.5 ± 0.9		
HT2h	3	11.1 ± 2.8	36.9 ± 2.9	10.8 ± 1.4	11.7 ± 0.2	12.7 ± 0.8	3.4	3.7
	14	5.9 ± 3.1	39.6 ± 7.1	9.9 ± 0.9	15.1 ± 1.2	16.4 ± 1.8		
HT24h	3	10.8 ± 1.4	34.7 ± 1.2	5.3 ± 1.9	17.4 ± 3.8	14.0 ± 0.9	4.4	5.9
	14	6.3 ± 1.4	37.2 ± 5.3	4.4 ± 2.2	21.8 ± 1.5	20.9 ± 1.6		

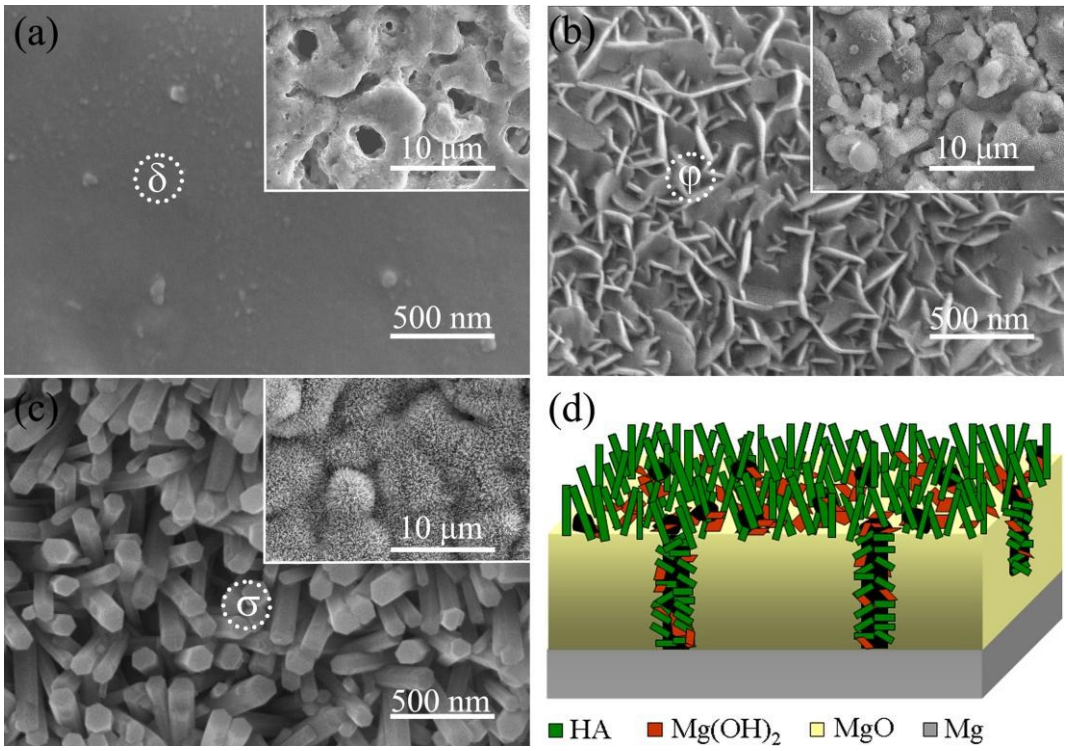

Fig. 1 Surface morphologies of (a) MAO_0, (b) HT2h (c) and HT24h coatings (the insets showing corresponding low-magnification images); (d) schematic architecture of HT24h-coated Mg. Elemental compositions at points σ, φ and δ in the images were detected by EDX and listed in Figs. 8e, S4c and S5c, respectively.

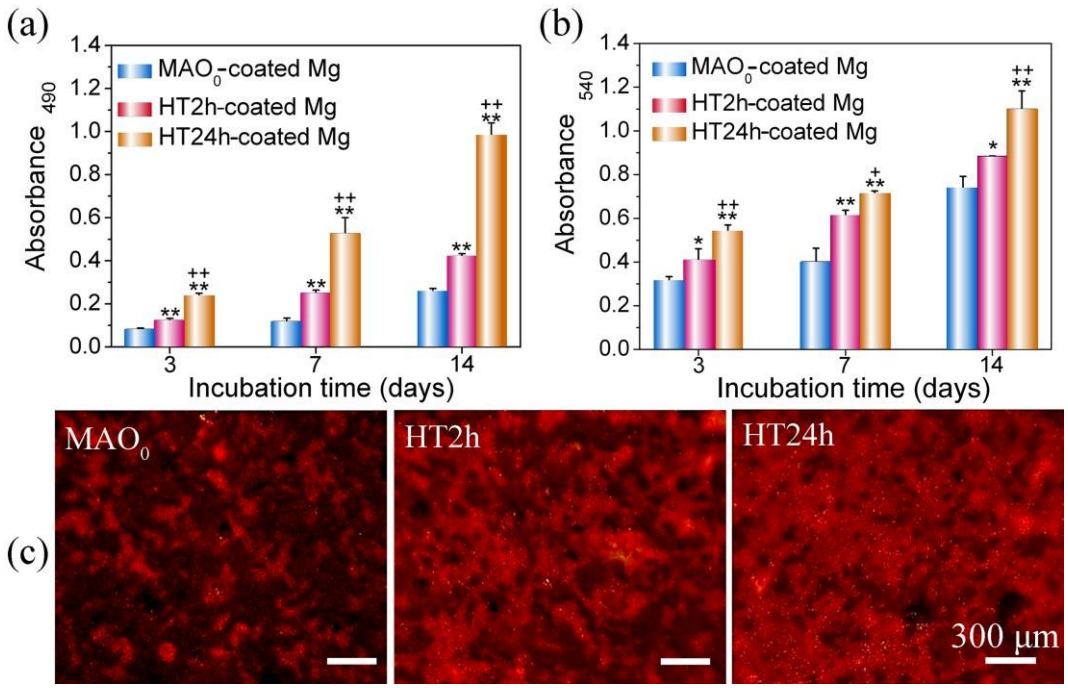

Fig. 2 (a) MTT assay of osteoblasts incubated on the coated Mg for 3, 7, and 14 days; (b) collagen secretion on MAO_0-, HT2h- and HT24h-coated Mg at days 3, 7, and 14 of incubation, and (c) staining pictures of collagen secretion at day 7. Data are presented as the mean ± SD, n = 4, (*) $p < 0.05$ and (**) $p < 0.01$ compared with MAO_0-coated Mg, (+) $p < 0.05$ and (++) $p < 0.01$ compared with HT2h-coated Mg.

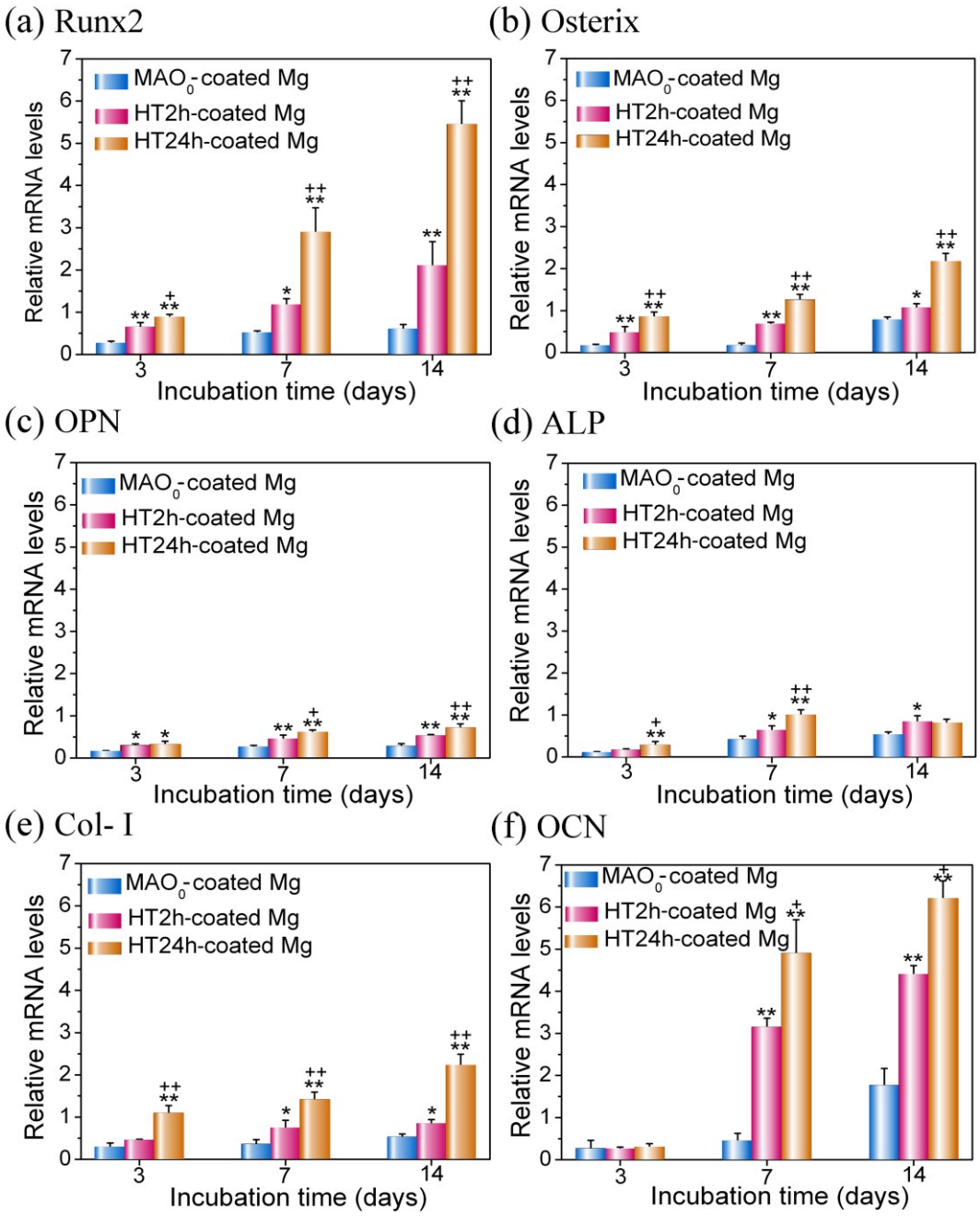

Fig. 3 Gene expressions of osteoblasts cultured on MAO_0-, HT2h- and HT24h-coated Mg after incubation of 3, 7, and 14 days: (a) Runx2; (b) osterix; (c) OPN; (d) ALP; (e) Col-I; (f) OCN. Data are presented as the mean ± SD, n = 4, (*) $p < 0.05$ and (**) $p < 0.01$ compared with MAO_0-coated Mg, (+) $p < 0.05$ and (++) $p < 0.01$ compared with HT2h-coated Mg.

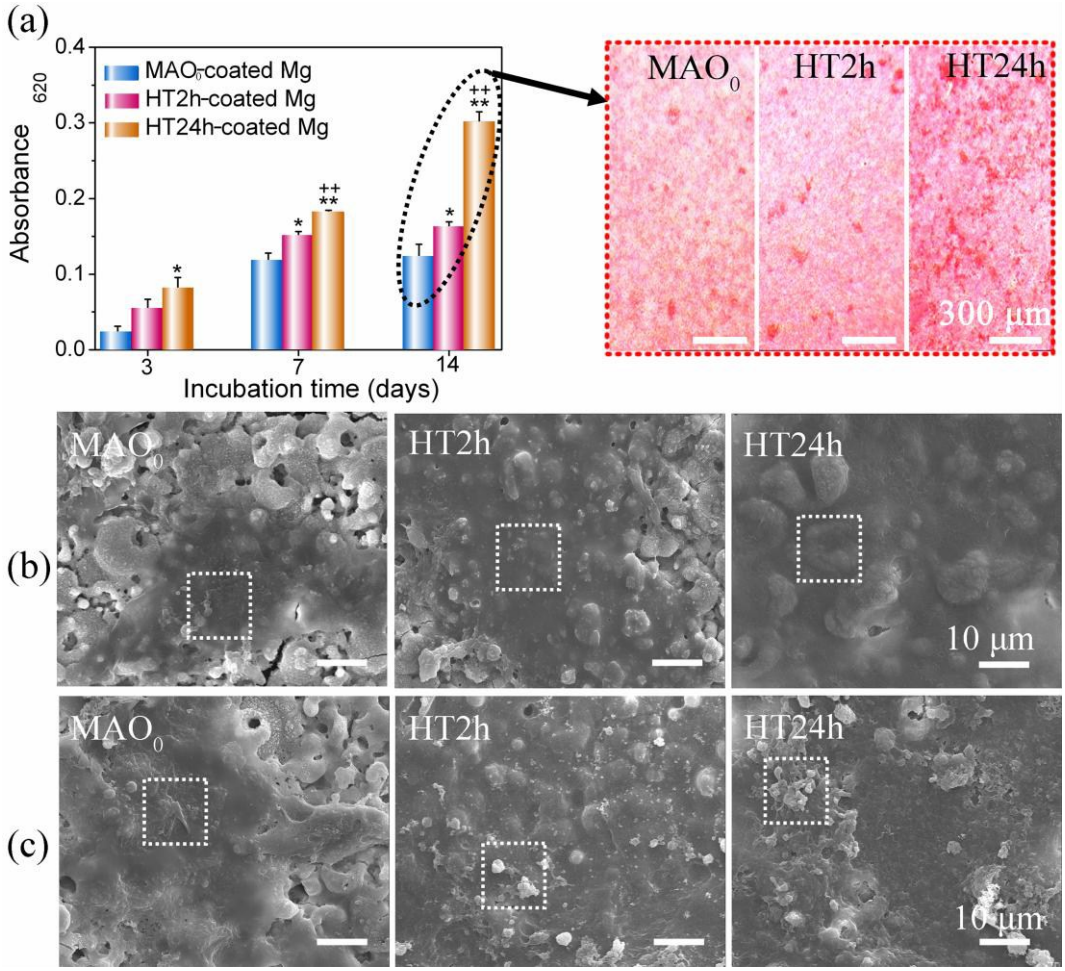

Fig. 4 ECM mineralization of osteoblasts on MAO_0-, HT2h- and HT24h-coated Mg: (a) Alizarin Red staining assessed quantitative values at days 3, 7, and 14 of incubation and the staining pictures taken at day 14 as a visual example; FE-SEM images of the osteoblasts cultured on the coated Mg for (b) 3 and (c) 14 days. Data are presented as the mean ± SD, n = 4, (*) $p < 0.05$ and (**) $p < 0.01$ compared with MAO_0-coated Mg, (+) $p < 0.05$ and (++) $p < 0.01$ compared with HT2h-coated Mg.

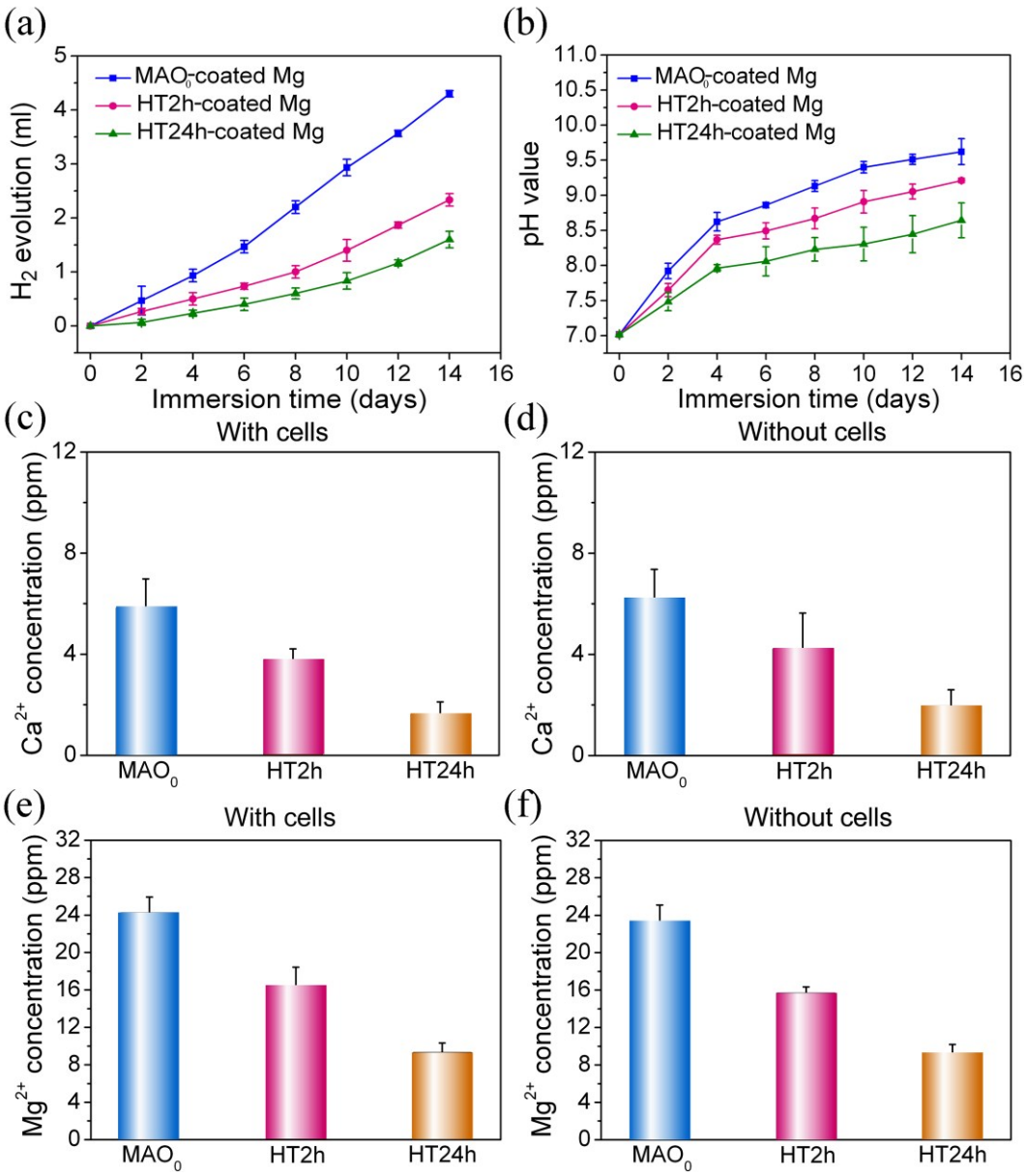

Fig. 5 (a) Hydrogen volumes released by MAO_0-, HT2h- and HT24h-coated Mg in serum-free culture medium, (b) pH values of serum-free culture medium immersing MAO_0-, HT2h- and HT24h-coated Mg as a function of immersion time, Ca^{2+} (c, d) and Mg^{2+} (e, f) concentrations of CCM immersing MAO_0-, HT2h- and HT24h-coated Mg seeded with (c, e) and without (d, f) osteoblasts after 1 day immersion.

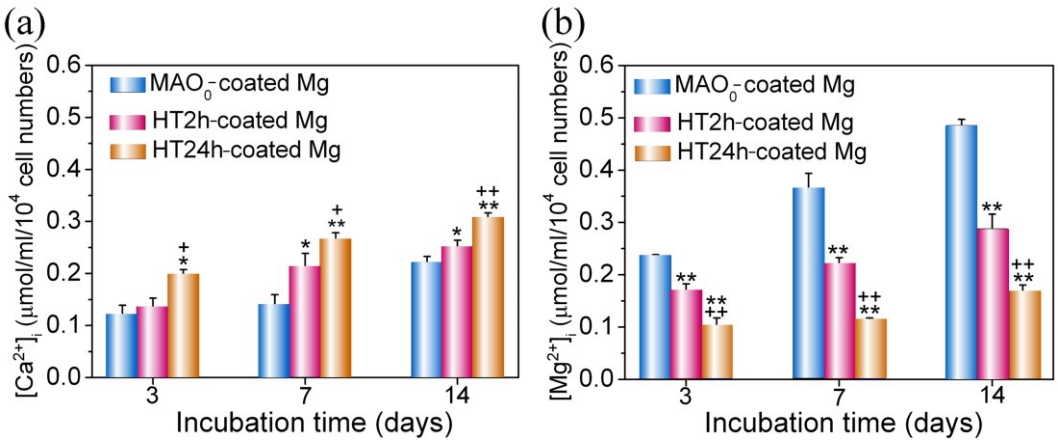

Fig. 6 (a) $[Ca^{2+}]_i$ and (b) $[Mg^{2+}]_i$ of osteoblasts cultured on MAO_0-, HT2h- and HT24h-coated Mg for 3, 7, and 14 days. Data are presented as the mean ± SD, n = 4, (*) $p < 0.05$ and (**) $p < 0.01$ compared with MAO_0-coated Mg, (+) $p < 0.05$ and (++) $p < 0.01$ compared with HT2h-coated Mg.

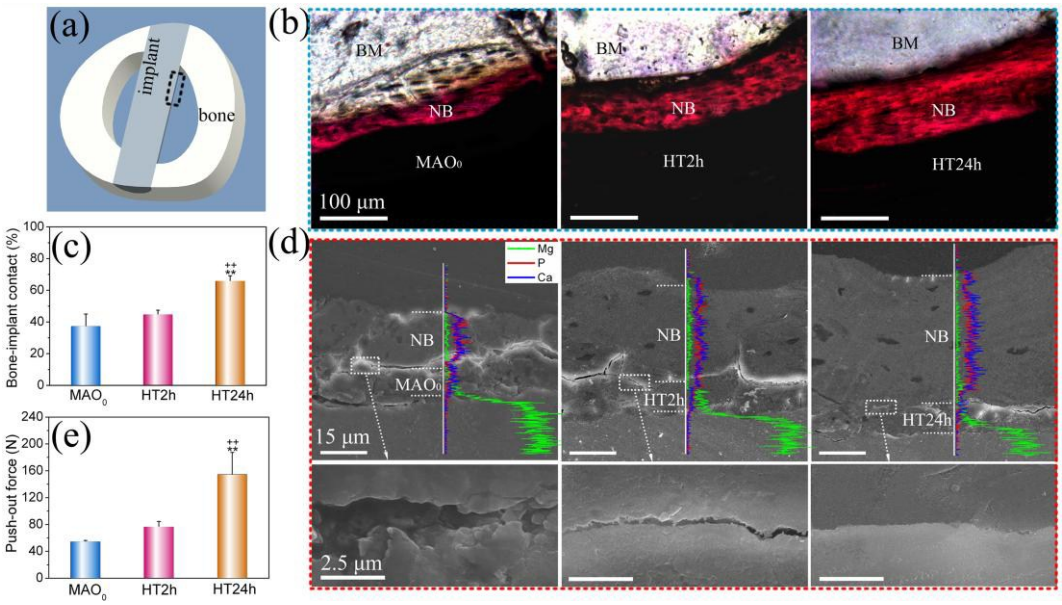

Fig. 7 (a) Schematic diagram showing the rectangle-marked region for histological analysis and FE-SEM observation of the coated pillar implanted in rabbit femur for 8 weeks. (b) Histological strained pictures; NB: new bone, BM: bone marrow. (c) Bone-implant contacts and (e) push-out forces of the coated Mg pillars. (d) Cross-sectional FE-SEM morphologies at the interfaces of new bones and the coated Mg pillars, together with the magnified images of the interfaces. Data are presented as the mean ± SD, n = 3, (**) $p < 0.01$ compared with MAO_0-coated Mg; (++) $p < 0.01$ compared with HT2h-coated Mg.

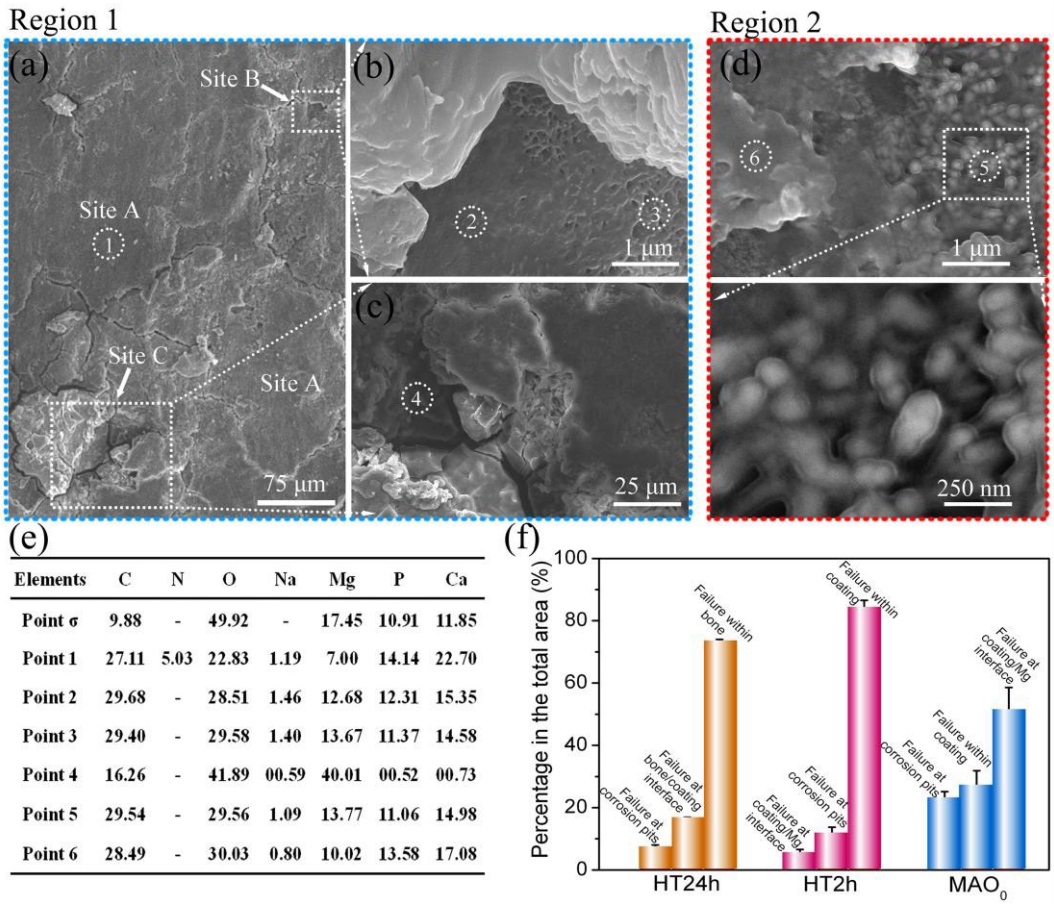

Elements	C	N	O	Na	Mg	P	Ca
Point σ	9.88	-	49.92	-	17.45	10.91	11.85
Point 1	27.11	5.03	22.83	1.19	7.00	14.14	22.70
Point 2	29.68	-	28.51	1.46	12.68	12.31	15.35
Point 3	29.40	-	29.58	1.40	13.67	11.37	14.58
Point 4	16.26	-	41.89	00.59	40.01	00.52	00.73
Point 5	29.54	-	29.56	1.09	13.77	11.06	14.98
Point 6	28.49	-	30.03	0.80	10.02	13.58	17.08

Fig. 8 FE-SEM surface morphologies and EDX-detected elemental compositions of the push-out disrupted surface on the side of HT24h-coated Mg pillar implanted in rabbit femur for 8 weeks: (a) image of region 1 on HT24h-coated pillar, and magnified images of (b) site B and (c) site C in (a); (d) image of region 2 on HT24h-coated pillar together with the magnified image of the dotted-square marked area. (e) listing the elements contents (at.%) detected at the points 1~6 marked in the above-mentioned images, together with that detected at point σ on HT24h shown in Fig. 1, (f**)** area percentage of the various failure modes in total area of each kind of the pushed-out surfaces on HT24h-, HT2h- and MAO_0-coated Mg pillars.